ChemComm

COMMUNICATION

View Article Online
View Journal | View Issue

Cite this: *Chem. Commun.*, 2020, **56**, 12965

Received 14th August 2020,
Accepted 15th September 2020

DOI: 10.1039/d0cc05556e

rsc.li/chemcomm

Kinetic and mechanistic analysis of a synthetic reversible CO_2/HCO_2^- electrocatalyst†

Drew W. Cunningham and Jenny Y. Yang *

$[Pt(depe)_2](PF_6)_2$ electrocatalyzes the reversible conversion between CO_2 and HCO_2^- with high selectivity and low overpotential but low rates. A comprehensive kinetic analysis indicates the rate determining step for CO_2 reduction is the reactivity of a Pt hydride intermediate to produce HCO_2^-. To accelerate catalysis, the use of cationic and hydrogen-bond donor additives are explored.

Photosynthesis utilizes solar energy to upgrade CO_2 to organic structural materials and chemical fuels. The prospect of replicating this feat in a synthetic system has driven interest in bio-inspired systems for carbon conversion schemes.[1] The two-electron oxidation of formate (HCO_2^-) to CO_2 is catalyzed in nature by the formate dehydrogenase (FDH) enzyme. A key feature of FDH is that it also catalyzes the reverse reaction, CO_2 reduction to formate.[2] Reversible catalysis is a hallmark of many redox enzymes and indicates catalysis is occurring with negligible overpotentials.[3]

We recently reported the reversible conversion between CO_2 and HCO_2^- by the synthetic electrocatalyst, $[Pt(depe)_2](PF_6)_2$ (**1**) where depe = 1,2-*bis*(diethylphosphino)ethane.[4] Complex **1** operates with high selectivity in both directions (>95% faradaic efficiency) and <50 mV of overpotential for CO_2 reduction. We previously noted the catalytic rate was too slow for reliable measurement by cyclic voltammetry (<0.5 s^{-1}). The slow rate of catalysis precludes **1** from being a faithful functional mimic of FDH.

In this study, detailed kinetic analyses of $[Pt(depe)_2](PF_6)_2$ (**1**) using electrochemical methods and stoichiometric reactions are described. The proposed catalytic cycle is shown in Scheme 1: Step A, $2e^-$ reduction of **1** to $Pt(depe)_2$ (**2**); (B) protonation to generate $[HPt(depe)_2]^+$ (**3**); and (C), CO_2 reduction to formate. The rate for a possible competitive side reaction (Step B′) was also considered. We note that we recently published a kinetic analysis on the similar catalyst, $[Pt(dmpe)_2](PF_6)_2$ (where dmpe = 1,2-bis(dimethylphosphino)ethane).[5] Although switching from methyl to ethyl substituents on the phosphine ligand is a subtle change, it results in the free energy for hydride transfer being nearly 4 kcal mol^{-1} more favorable for the methyl-containing variant $[HPt(dmpe)_2]^+$. This minor modification leads to important differences in their reactivities; notably $[Pt(dmpe)_2](PF_6)_2$ is not a reversible catalyst.

The studies on $[Pt(depe)_2](PF_6)_2$ (**1**) reveal that Step C, the reaction of $[HPt(depe)_2]^+$ (**3**) with CO_2 to regenerate **1** and HCO_2^- is likely the rate-determining step (RDS) for catalysis. Sluggish reactivity at metal hydride intermediates is common for CO_2 to HCO_2^- electrocatalysts. There are only a few known homogeneous electrocatalysts with high selectivity for HCO_2^- (>90% faradaic efficiency). In addition to $[Pt(depe)_2](PF_6)_2$ (**1**) and $[Pt(dmpe)_2](PF_6)_2$,[6] an Fe carbonyl cluster from Berben *et al.*,[7] two Ir complexes from Brookhart and Meyer *et al.*[8] and Berskoetter, Hazari, Palmore *et al.*,[9] and a Co complex from

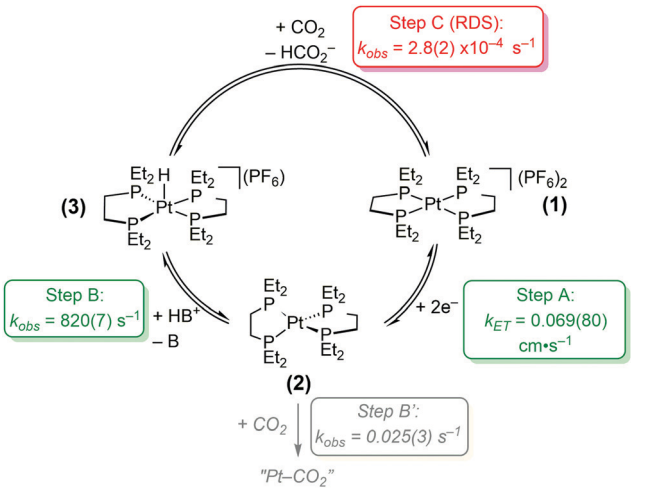

Scheme 1 Proposed catalytic cycle and corresponding rates of reactions for electrocatalytic CO_2 reduction to HCO_2^- by $[Pt(depe)_2](PF_6)_2$ (1). Conditions: 5 mM 1, 100 mM $CH_2(TBD)_2{\cdot}HPF_6$, 1 atm CO_2.

Department of Chemistry, University of California, Irvine, 92617, USA.
E-mail: j.yang@uci.edu

† Electronic supplementary information (ESI) available. See DOI: 10.1039/d0cc05556e

Artero *et al.*[10] have been reported. For all of these catalysts, the reaction of a metal hydride intermediate and CO_2 to produce formate is proposed to be the rate-determining step.

Although it is evident that the reaction of a metal hydride with CO_2 is a key step in formate production, there have been few experimental studies on the nature of the transition state for electrocatalysts. However, mechanistic studies on CO_2 hydrogenation catalysts and the enzyme formate dehydrogenase suggest the addition of secondary sphere cations[11] or hydrogen-bond donors[12] could accelerate this step. We explore the use of these additives and discuss the information they provide on the transition state.

Electron transfer rate constant. Upon reduction, $[Pt(depe)_2](PF_6)_2$ (**1**) exhibits a 2 e^- reversible redox event at −1.64 V *vs.* $Fc^{+/0}$ (where Fc = $Fe(C_5H_5)_2$). The electron transfer rate constant, k_{ET}, was determined using the Butler–Volmer method,[13] which is described in more detail in the ESI.† The scan rate dependent cyclic voltammetry is shown in Fig. S1 and S2 (ESI†). Using this method, the $2e^-$ k_{ET} is 0.069(80) cm s^{-1}.

Reactivity of [Pt(depe)$_2$] (2) with H$^+$ vs. CO$_2$. Under electrocatalytic conditions, the reduced intermediate $[Pt(depe)_2]$ (**2**) can either react with CO_2 or the proton source $CH_2(TBD)_2{\cdot}HPF_6$ where TBD = triazabicyclodecene (pK_a = 29 in CH_3CN).[14] The direct reaction of CO_2 with reduced metal centers typically leads to a metal carboxylate.[15] The metal carboxylate can either protonate twice to generate CO and H_2O or disproportionate with another equivalent of CO_2 to give CO and CO_3^{2-}. Conversely, direct protonation at a reduced metal center results in formation of a metal hydride as proposed in our catalytic cycle. To explore both these possibilities, we investigated the independent reactivity of electrochemically generated $[Pt(depe)_2]$ with either CO_2 or H^+.

Protonation of [Pt(depe)$_2$] (2). In the absence of CO_2, the stoichiometric reaction of $[Pt(depe)_2]$ (**2**) with $CH_2(TBD)_2{\cdot}HPF_6$ was previously shown by $^{31}P\{^1H\}$ NMR to give $[HPt(depe)_2]^+$ (**3**) (Scheme 1). Thus, we would expect electrochemically-generated **2** to protonate and generate **3** *in situ*. The cyclic voltammograms of **1** in the presence of H^+ under 1 atm N_2 retain the expected cathodic peak associated with reduction to **2**. However, the anodic peak is only present at higher scan rates (Fig. 1). At more cathodic potentials, a feature appears at *ca.* −2.9 V *vs.* $Fc^{+/0}$ (Fig. S3, ESI† blue trace), which is attributed to the subsequent reduction of $[HPt(depe)_2]^+$ (**3**). The reduction at −2.9 V *vs.* $Fc^{+/0}$ is only present with the addition of acid. CVs of independently-isolated **3** have the same irreversible feature (Fig. S3, ESI† red trace), confirming generation of $[HPt(depe)_2]^+$ (**3**) upon reduction in the presence of $CH_2(TBD)_2{\cdot}HPF_6$.[4]

The rate constant for protonation of the electrogenerated reduced platinum species, **2**, was investigated using scan-rate dependent cyclic voltammetry (Fig. 1 and Fig. S4, S5, ESI†). As expected for an EEC reaction ($2e^-$ transfer followed by a chemical step), the cathodic peak potentials shift to more negative values at higher scan rates (Fig. 1 inset, and Fig. S4, S5, ESI†). Additionally, at slower scan rates, the return oxidation wave is almost completely diminished due to consumption of electrogenerated **2** to form **3**. At faster scan rates, almost complete reversibility is achieved as re-oxidation of **2** outcompetes protonation. Analysis of the cathodic peak shift[16] (see ESI†) with 10 mM of $CH_2(TBD)_2{\cdot}H^+$ results in an observed rate constant for protonation, or k_{obs} of 74(11) s^{-1}.

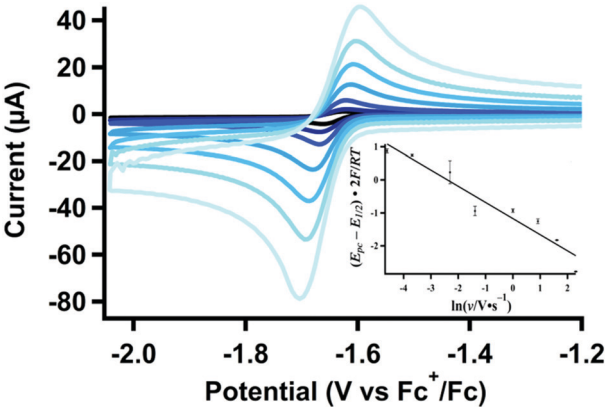

Fig. 1 Variable scan-rate CVs (0.025–10 V s^{-1}) of $[Pt(depe)_2](PF_6)_2$ (**1**) (1.06 mM) with $CH_2(TBD)_2{\cdot}HPF_6$ (5.00 mM) and (b) linear plot for the change in cathodic peak potential used for calculating $k_{obs,H+}$. Additional data used for calculation shown in Fig. S1 and S2 (ESI†).

The dependence of acid concentration on observed rate confirmed that protonation is first order in acid (Fig. S6, ESI†). The observed rate constants for protonation of **2** are 36(4) and 54(10) s^{-1} for 5.0 and 7.5 mM $CH_2(TBD)_2{\cdot}H^+$, respectively, and the 2nd order rate constant is 8.2(7) × 10^3 M^{-1} s^{-1}. Thus, the k_{obs} under catalytic conditions with 100 mM $CH_2(TBD)_2{\cdot}H^+$ is 820(7) s^{-1}, indicating protonation of **2** is relatively facile.

Reactivity of [Pt(depe)$_2$] (2) and CO$_2$. Reduction of $[Pt(depe)_2](PF_6)_2$ (**1**) under 1 atm CO_2 and aprotic conditions leads to the loss of reversibility of the Pt(II/0) couple, suggesting the electrogenerated $[Pt(depe)_2]$ (**2**) can also react with CO_2. We observed similar reactivity with the related compound $[Pt(dmpe)_2]$. The loss of reversibility is scan-rate dependent (Fig. S7–S9, ESI†); at faster scan rates the current associated with re-oxidation of **2** to **1** increases. The electrochemical peak current analysis used to derive the rate of protonation (*vide supra*) could not be used for this reaction because the cathodic shifts are too small (indicating a slow rate). An alternative method was used to determine the rate. Analysis of the ratio between the anodic return current *vs.* the initial cathodic current (i_{pa}/i_{pc})[17] at different scan rates provides a half-life for the reaction of 26 s^{-1}, which corresponds to a pseudo first-order CO_2 binding rate constant, k_{CO_2}, of 0.027 s^{-1}. The data indicate that while the reaction between **2** and CO_2 is favorable in the absence of protons, the rate constant is 10^5 slower than the rate at which **2** is protonated under catalytic conditions. Thus the direct reactivity of CO_2 with **2** is negligible during catalysis.

Hydride transfer step. $[HPt(depe)_2]^+$ (**3**) was independently synthesized and isolated. We previously demonstrated that hydride transfer from **3** to CO_2 proceeds cleanly without any side products or reactions. The generation of HCO_2^- was quantified using ^1H NMR spectroscopy. The quantity of HCO_2^- at each time point was subtracted from the initial concentration of **3** to deduce the concentration of **3** at each time point

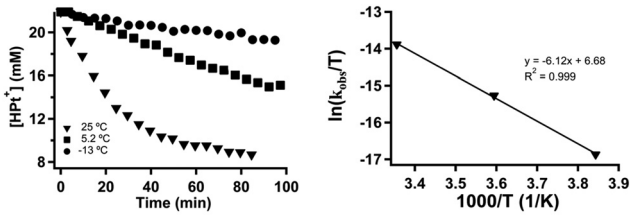

ΔH‡ (kcal/mol)	ΔS‡ (cal/mol)	ΔG‡ (298K, kcal/mol)
12	-34	22

Fig. 2 For the reaction of $[HPt(depe)_2]^+$ (**3**) (21.9 mM) with CO_2 (1.0 atm) (top left) concentrations of **3** over time at various temperatures, (top right) corresponding Eyring plot, and (bottom) activation parameters.

(Fig. 2). The rate constant, k_{obs}, was calculated to be 2.78(17) × 10^{-4} s^{-1} using initial rates (see ESI†). Initial rates were used because the reaction has a K_{eq} of 1.05(7) and approaches equilibrium over time.[4]

To determine more information about the nature of the transition state, the activation parameters were calculated by measuring the rates at variable temperatures (Fig. 2). The observed rate constants for the reactions at 5 and −13 °C are 6.52(21) × 10^{-5} s^{-1} and 1.23(4) × 10^{-5} s^{-1}, respectively. As expected, the rates are significantly slower than the reactions at 25 °C. From the Eyring plot (Fig. 2b) the activation parameters are: $\Delta H^{\ddagger}$ = 12.2(4) kcal mol^{-1}, $\Delta S^{\ddagger}$ = −34(1) cal mol^{-1} K, and $\Delta G^{\ddagger}_{298K} = 22.3(1)$ kcal mol^{-1}. As anticipated, the large $\Delta G^{\ddagger}_{298K}$ term suggests sluggish kinetics at room temperature. The entropic term suggests a large degree of order in the transition state and is consistent with a bimolecular reaction between two species and is in agreement with the few reported activation parameters for hydride transfer to CO_2.[11]

Rate determining step. Understanding the heterogenous electron transfer rate constant with respect to chemical steps is not inherently intuitive. However, we can compare overall electrocatalytic rates and proposed RDS of catalysts that have slower rates of electron transfer than **1**. $[Fe_4N(CO)_{12}]^-$ is an electrocatalyst for CO_2 reduction to HCO_2^- and operates with a fast turnover frequency (TOF) of 210 s^{-1}.[7d] The RDS for this catalyst is hydride transfer to CO_2, not electron transfer. A Co diphosphine H_2 evolution catalyst that operates with a TOF of 160 s^{-1} has a k_{ET} = 0.003 cm s^{-1}.[18] For this particular catalyst, protonation of the reduced Co(I) species to generate the metal hydride is proposed to be rate-limiting.[18b] The measured k_{ET} values in these examples are an order of magnitude slower than **1** and have TOFs in the 100s. The rates of our last proposed chemical step, C, has a k_{obs} of 2.78(17) × 10^{-4} s^{-1}. From these comparisons, we conclude that the 2 e^- reduction of **1** to generate **2** is not rate-limiting. Step C is also significantly slower than our measured rate for step B (protonation to generate the Pt hydride), and is therefore likely the rate-determining step. The slow rate measured for step C is consistent with the small catalytic current we observe for CO_2 reduction to HCO_2^-.[4]

Accelerating proposed RDS. To date, intimate mechanistic details for the insertion of CO_2 into metal hydrides bonds are lacking and mostly based on computational studies.[19] Two of

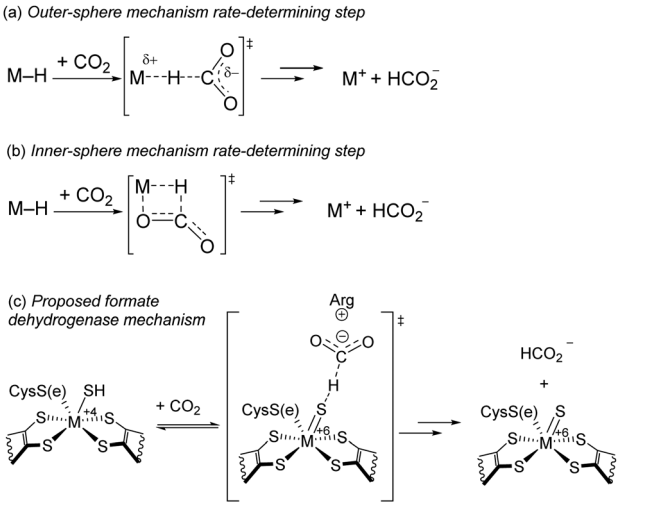

Scheme 2 (a and b) Common mechanisms for CO_2 Insertion into metal hydrides described in ref. 11, (c) proposed mechanism for hydride transfer in formate dehydrogenase described in ref. 12.

the most commonly proposed mechanisms for CO_2 insertion are shown in Scheme 2a and b.[11] In the (a) outer-sphere mechanism, a hydride is delivered directly to CO_2 with concomitant cleavage of the M–H and C–H bond formation. In the (b) inner-sphere mechanism, M–H and CO_2 join in a side-on fashion giving rising to a metallocyclic transition state. Both mechanisms have a large negative entropy of activation, so they are not distinguishable by our Eyring parameters. Hazari and colleagues studied the kinetics of CO_2 insertion into various metal hydrides.[11,20] They found the rate of the reaction between CO_2 and an Ir pincer trihydride complex and $[HRu(tpy)(bpy)](PF_6)$ can be accelerated by up to a factor of $\times 10^3$ upon addition of salts, particularly Lewis acidic (LA) cations.[11] In these cases, it is believed hydride transfer follows an outer-sphere mechanism, and the acceleration in rate is due to stabilization of the negative charge on the carboxylate moiety in the transition state. In the case of a Ni pincer hydride complex, no enhancement was observed, leading the authors to conclude the reaction likely follows an inner-sphere mechanism.

In the most recent proposed mechanism of the enzyme formate dehydrogenase, hydride transfer resembles an outer-sphere approach (Scheme 2c).[12] In metal-dependent formate dehydrogenation enzymes, a conserved arginine residue near the active site is critical for catalytic activity. With a pK_a of 12.5, arginine is expected to be protonated under biological conditions. In this mechanism, a cationic protonated arginine in the secondary coordination sphere is proposed to stabilize the carboxylate species through hydrogen-bonding and/or electrostatic interactions.

In an attempt to accelerate the rate of CO_2 insertion into **3**, lithium bis(trifluoromethane)sulfonimide ($LiNTf_2$) was added to the reaction. We selected $LiNTf_2$ because of its relatively high solubility in acetonitrile and because it exhibited the highest rate acceleration for the previously reported iridium pincer trihydride complex.[11b] UV-Visible spectroscopy (UV-Vis) was used to quantify the rate instead of ^1H NMR measurements

in the presence of $LiNTf_2$ due to precipitation of lithium formate at the mM concentrations required for NMR (Fig. S10, ESI†). Using the method of initial rates (data for $t < 20$ min) and a lower concentration of **1** (0.100 mM) the rate was $6.50(7) \times 10^{-5}$ s^{-1} without $LiNTf_2$ and $7.23(6) \times 10^{-5}$ s^{-1} with 10 mM $LiNTf_2$. Thus, the addition of $LiNTf_2$ does not significantly increase the rate of CO_2 reactivity with **3**.

To mimic the role of a protonated arginine, guanidinium tetraphenylborate was also tested as an additive to accelerate reactivity. Guanidinium (pK_a of 23.3 in CH_3CN) is a stronger proton donor than the $CH_2(TBD)_2{\cdot}HPF_6$ we normally use for catalysis.[21] Fig. S12 (ESI†) shows the CVs with addition of guanidinium·BPh_4. Upon addition of guanidinium·BPh_4, the anodic (return) wave diminishes after reduction, consistent with protonation of $[Pt(depe)_2]$ (**2**) to form $[HPt(depe)_2]^+$ (**3**). The addition of CO_2 leads to a reduction in cathodic current, which is recovered with addition of excess guanidinium·BPh_4. However, the peak current does not increase with the addition of guanidinium·BPh_4.

As neither $LiNTf_2$ nor guanidinium·BPh_4 increase the rate of the proposed RDS or catalysis, we conclude that Step C likely proceed through an inner-sphere mechanism (Scheme 2b). An inner-sphere mechanism was previously attributed to a Ni pincer hydride complex as various additives did not significantly affect the rate of CO_2 insertion.[11a] This mechanism may consist of several elementary steps to produce HCO_2^-, although we expect any potential intermediates are likely short-lived. We have observed no catalyst-based intermediates from **3** to **2**.

Currently, all of the evidence for reported CO_2 reduction to HCO_2^- electrocatalysts indicate the rate limiting step is the reaction of a metal hydride with CO_2. Understanding the different possible mechanisms, the metal hydride properties that make each mechanism favorable, and how each mechanism can be accelerated through synthetic design or reaction conditions would make a profound impact on developing new catalysts. As our understanding of metal hydride reactivity progresses, we can aspire to new synthetic catalysts that replicate the selectivity, low overpotential, and speed of enzymes.

This study was supported by the US Department of Energy, Office of Science, Office of Basic Energy Sciences Award DE-SC0012150 and DE-0000243266. J. Y. Y. acknowledges support as a Sloan Foundation Fellow, Canadian Institute for Advanced Research (CIFAR) Azrieli Global Scholar in the Bio-Inspired Solar Energy Program, and a Camille Dreyfus Teacher-Scholar.

Conflicts of interest

There are no conflicts to declare.

Notes and references

1 (*a*) H. B. Gray, *Nat. Chem.*, 2009, **1**, 7; (*b*) N. S. Lewis, *Science*, 2007, **315**, 798–801; (*c*) N. S. Lewis and D. G. Nocera, *Proc. Natl. Acad. Sci. U. S. A.*, 2006, **103**, 15729–15735.
2 T. Reda, C. M. Plugge, N. J. Abram and J. Hirst, *Proc. Natl. Acad. Sci. U. S. A.*, 2008, **105**, 10654–10658.
3 (*a*) J.-M. Savéant, *ACS Catal.*, 2018, **8**, 7608–7611; (*b*) F. A. Armstrong and J. Hirst, *Proc. Natl. Acad. Sci. U. S. A.*, 2011, **108**, 14049–14054.
4 D. W. Cunningham, J. M. Barlow, R. S. Velazquez and J. Y. Yang, *Angew. Chem., Int. Ed.*, 2020, **59**, 4443–4447.
5 B. M. Ceballos and J. Y. Yang, *Organometallics*, 2020, **39**, 1491–1496.
6 B. M. Ceballos and J. Y. Yang, *Proc. Natl. Acad. Sci. U. S. A.*, 2018, **115**, 12686–12691.
7 (*a*) A. Taheri, E. J. Thompson, J. C. Fettinger and L. A. Berben, *ACS Catal.*, 2015, **5**, 7140–7151; (*b*) N. D. Loewen, T. V. Neelakantan and L. A. Berben, *Acc. Chem. Res.*, 2017, **50**, 2362–2370; (*c*) A. Taheri and L. A. Berben, *Inorg. Chem.*, 2016, **55**, 378–385; (*d*) A. Taheri, C. R. Carr and L. A. Berben, *ACS Catal.*, 2018, **8**, 5787–5793.
8 (*a*) P. Kang, C. Cheng, Z. Chen, C. K. Schauer, T. J. Meyer and M. Brookhart, *J. Am. Chem. Soc.*, 2012, **134**, 5500–5503; (*b*) P. Kang, T. J. Meyer and M. Brookhart, *Chem. Sci.*, 2013, **4**, 3497–3502.
9 S. T. Ahn, E. A. Bielinski, E. M. Lane, Y. Chen, W. H. Bernskoetter, N. Hazari and G. T. R. Palmore, *Chem. Commun.*, 2015, **51**, 5947–5950.
10 S. Roy, B. Sharma, J. Pécaut, P. Simon, M. Fontecave, P. D. Tran, E. Derat and V. Artero, *J. Am. Chem. Soc.*, 2017, **139**, 3685–3696.
11 (*a*) J. E. Heimann, W. H. Bernskoetter and N. Hazari, and James M. Mayer, *Chem. Sci.*, 2018, **9**, 6629–6638; (*b*) J. E. Heimann, W. H. Bernskoetter and N. Hazari, *J. Am. Chem. Soc.*, 2019, **141**, 10520–10529.
12 L. B. Maia, L. Fonseca, I. Moura and J. J. G. Moura, *J. Am. Chem. Soc.*, 2016, **138**, 8834–8846.
13 J. M. Savéant, *Investigation of Rates and Mechanisms of Reactions*, Wiley, 1986, ch. 7.
14 I. Kaljurand, J. Saame, T. Rodima, I. Koppel, I. A. Koppel, J. F. Kögel, J. Sundermeyer, U. Köhn, M. P. Coles and I. Leito, *J. Phys. Chem. A*, 2016, **120**, 2591–2604.
15 J. M. Barlow and J. Y. Yang, *ACS Cent. Sci.*, 2019, **5**, 580–588.
16 J. M. Savéant, *Elements of Molecular and Biomolecular Electrochemistry: An Electrochemical Approach to Electron Transfer Chemistry*, Wiley, 2006.
17 (*a*) J. Y. Yang, R. M. Bullock, W. J. Shaw, B. Twamley, K. Fraze, M. R. DuBois and D. L. DuBois, *J. Am. Chem. Soc.*, 2009, **131**, 5935–5945; (*b*) J. M. Saveant, *Investigation of Rates and Mechanisms of Reactions*, Wiley, 1986.
18 (*a*) E. S. Wiedner, J. Y. Yang, W. G. Dougherty, W. S. Kassel, R. M. Bullock, M. R. DuBois and D. L. DuBois, *Organometallics*, 2010, **29**, 5390–5401; (*b*) E. S. Wiedner and R. M. Bullock, *J. Am. Chem. Soc.*, 2016, **138**, 8309–8318.
19 (*a*) W. H. Bernskoetter and N. Hazari, *Eur. J. Inorg. Chem.*, 2013, 4032–4041; (*b*) F. Huang, C. Zhang, J. Jiang, Z.-X. Wang and H. Guan, *Inorg. Chem.*, 2011, **50**, 3816–3825; (*c*) Q.-Q. Ma, T. Liu, A. Adhikary, J. Zhang, J. A. Krause and H. Guan, *Organometallics*, 2016, **35**, 4077–4082; (*d*) I. Osadchuk, T. Tamm and M. S. G. Ahlquist, *Organometallics*, 2015, **34**, 4932–4940; (*e*) P. Ríos, A. Rodríguez and J. López-Serrano, *ACS Catal.*, 2016, **6**, 5715–5723; (*f*) T. J. Schmeier, G. E. Dobereiner, R. H. Crabtree and N. Hazari, *J. Am. Chem. Soc.*, 2011, **133**, 9274–9277; (*g*) T. J. Schmeier, N. Hazari, C. D. Incarvito and J. A. Raskatov, *Chem. Commun.*, 2011, **47**, 1824–1826; (*h*) H.-W. Suh, T. J. Schmeier, N. Hazari, R. A. Kemp and M. K. Takase, *Organometallics*, 2012, **31**, 8225–8236.
20 N. Hazari and J. E. Heimann, *Inorg. Chem.*, 2017, **56**, 13655–13678.
21 Z. Glasovac, M. Eckert-Maksić and Z. B. Maksić, *New J. Chem.*, 2009, **33**, 588–597.

